Research Square

Preprints are preliminary reports that have not undergone peer review.
They should not be considered conclusive, used to inform clinical practice,
or referenced by the media as validated information.

Study on Formation Kinetics and Mechanism of Barium-Calcium Phosphoaluminate Mineral

Jungang Yuan
University of Jinan
Hao Liu
China Railway Construction Engineering Group Shandong Co.
Fengnian Wu
University of Jinan
Yongbo Huang
University of Jinan
Jinghua Yan
University of Jinan
Shoude Wang (13589047192@163.com)
University of Jinan
Lingchao Lu
University of Jinan

Research Article

Keywords: Calcination temperature, Conversion rate, Determination coefficient, Reaction rate, Activation energy

Posted Date: January 4th, 2022

DOI: https://doi.org/10.21203/rs.3.rs-1222937/v1

License: This work is licensed under a Creative Commons Attribution 4.0 International License.
Read Full License

Abstract

Barium-calcium phosphoaluminate ($(C,B)_8A_6P$) mineral was synthesized by introducing Ba^{2+} into the lattice of calcium phosphoaluminate (C_8A_6P) mineral and it owned the better hydration activity than C_8A_6P. In this study, the formation kinetics and mechanism of $(C,B)_8A_6P$ mineral was firstly systematically explored. The experimental results indicated that calcination temperature had a significant effect on the formation of $(C,B)_8A_6P$ mineral. The conversion rate of $(C,B)_8A_6P$ mineral was less than 0.5 and reaction rate was less than 9.4×10^{-7} with the holding time of 8 h at 1500-1530 °C. Nevertheless, the conversion rate and reaction rate reached 0.8 and 9.4×10^{-7}, respectively, with the holding time of only 2 h when the calcination temperature ranged from 1540 °C to 1560 °C. In addition, the Jander equation was feasible for the formation of $(C,B)_8A_6P$ with activation energy of 1310 kJ • mol^{-1} at 1500-1530 °C, while the Ginstling equation was feasible for use with activation energy of 324 kJ • mol^{-1} when the calcination temperature ranged from 1540 to 1560 °C.

1. Introduction

The production of Portland cement (PC) is accompanied with the high energy consumption and high pollution. It is considered that per ton of clinker contributed to about 3100MJ of heat energy consumption and 0.83 ton of carbon dioxide emission on average, which led to global warming, the so-called "green house effect"[1–4]. Furthermore, PC has been gradually unable to meet the requirements of modern high-standard engineering construction due to its some disadvantages such as low early strength [5], poor durability [6], terrible volume stability [7], etc. In order to acquire long service life [8], i.e. the time during which the constructions are capable of fulfilling its function without bigger reconstruction interventions in special engineering such as harbor bridge, oil well, tunnel, marine nuclear power plants, etc, cement scientists set out to pay attention to the research and development of special cement while improving the performance of PC [9–13].

Since the 1970s, the rapid hardening sulphoaluminate cement (SAC) with $3CaO • 3Al_2O_3 • CaSO_4$ as the main mineral has been widely produced and applied [14]. Based on this, $3CaO • 3Al_2O_3 • BaSO_4$ and $3CaO • 3Al_2O_3 • SrSO_4$ was synthesized, and the cementitious properties of which was better than $3CaO • 3Al_2O_3 • CaSO_4$ [15]. Feng [16] synthesized $3CaO·3Al_2O_3·SrSO_4$ single crystal with a size of 60~120 μm for the first time and obtained a full set of structural parameters through analysis. Yan [17]studied the hydration of calcium sulphoaluminate minerals containing Sr and Ba in the presence of sulfate. Then, a series of high-strength barium-calcium sulfoaluminate mineral $(3-x)CaO • xBaO • 3Al_2O_3 • CaSO_4$ ($C_{4-x}B_xA_3\$$) were synthesized and characterized, the mineralogical composition of which with the optimum mechanical properties was determined, and the cement with the $C_{2.75}B_{1.25}A_3\$$ as the main mineral was invented [18–20]. Furthermore, Cheng et al. [20][21] firstly synthesized and produced barium-calcium sulphoaluminate cement with excellent performance by using industrial waste containing barium.

In order to further improve the mechanical property and hydration characteristics of PAC, inspired by the sintering of barium-calcium sulphoaluminate mineral ($C_{4-x}B_xA_3\$$) with an energy of 227.45 kJ mol^{-1} at elevated temperatures ranged from 1300 to 1380°C [20–22], BaO was introduced into PAC system to modify mineral structure. PAC can obtain the higher compressive strength with the substitution mole ratio of BaO to CaO of 10.5 mol%, which was concluded that Ba^{2+} activated crystal structure of PAC and improved the hydration activity [23]. Other studies indicated that BaO of 17.5-20% content endowed calcium phosphoaluminate (C_8A_6P, predominant mineral of PAC) excellent mechanical performance [24].

In this article, Ba^{2+} was introduced into C_8A_6P lattice and substitute part of Ca^{2+} located at lattice particle position to form $(C,B)_8A_6P$ mineral. During the process of sintering the barium-calcium phosphoaluminate cement clinker, the thermal process system shows significant influence on the phosphoaluminate mineral formation [25], which mostly determined the quality of the clinker. Besides, the study of reaction mechanism and activation energy of solid phase will be of guiding significance to the preparation and application of barium-calcium phosphoaluminate cement. Therefore, it is essential to provide a deep understanding of the formation dynamics for the $(C,B)_8A_6P$ mineral.

2. Preparation And Testing

2.1 Sample preparation

Specimens were synthesized with reagents such as $CaCO_3$, $Ca_3(PO_4)_2$, SiO_2, $BaCO_3$, Al_2O_3, and Fe_2O_3 (Sinopharm Chemical Reagent Co., Ltd, China). The chemical reagents were weighed accurately according to the oxide component of barium-calcium phosphoaluminate. The materials were mixed and milled to obtain the raw meal. The raw meal was mixed with a small amount of distilled water and pressed into discs with a diameter of 60 mm and a height of 10 mm for sintering. Then, the discs were dried in an oven at 105°C for 2 h and sintered in a resistance furnace with a heating-up velocity of 5°C/min to specified temperature (1500, 1510, 1520, 1530, 1540, 1550 and 1560°C) for different holding time (2, 4, 6 and 8 h). Finally, the clinker was removed from resistance furnace, air-cooled sharply to room temperature, and ground to specified fineness.

2.2 Characterization

The internal standard method [26, 27] was adopted to determine conversion rate in this experiment. Internal standard method is a more accurate quantitative method in chromatographic analysis and is more advantageous especially when there is no reference substance. In this experiment, 20 ωt%, 40 ωt%, 60 ωt% and 80 ωt% standard specimen was mixed with 40 ωt% ZnO for XRD analysis. XRD analysis were performed by using A Bruker D8 X-ray diffractometer with Cu Kα radiation (λ = 0.15046 nm) under 40 kV and 40 mA. The data were collected from 5° to 70° with a rate of 0.2°/step and 5 step/s. Then, the peak areas (or peak intensity) and relative correction factor of internal standard substance and specimens to be measured were determined respectively, whose percentage content in the mixtures could be calculated according to the following equation:

$$\frac{I_A}{I_S} = K \times W_A$$

where I_A, I_S, K and W_A is the diffraction peak intensity of specimens, the diffraction peak intensity of internal standard substance (ZnO), the slope of the standard curve and the mass fraction of specimens in the mixtures, respectively.

3. Results And Discussions

3.1 Conventional solid-state kinetic reaction model

In solid-phase dynamics, a rational dynamic model was adopted to describe the reaction mechanism, which can be also intuitively reflected from the corresponding dynamics equation [28][29]. The common equations of dynamic mechanism and model of solid-state reaction were listed in Table 1.

Table 1

Reaction mechanism and dynamics equations for Different Reaction Models [22, 30, 31]

Model	Dynamics equation	Reaction mechanism	Model type
Avrami–Erofeyev (A_2)	$[-\ln(1-\alpha)]^{1/2}=kt$	Nucleation and growth	
Avrami–Erofeyev (A_3)	$[-\ln(1-\alpha)]^{1/3}=kt$		
Avrami–Erofeyev (A_4)	$[-\ln(1-\alpha)]^{1/4}=kt$		
2-D diffusion (D_2)	$(1-\alpha)\ln(1-\alpha)+\alpha=kt$	Diffusion Mechanism	Cylindrical model
3-D diffusion–Jander (D_3)	$[1-(1-\alpha)^{1/3}]^2=kt$		Spherical model
Ginstling–Brounshtein (D_4)	$[1-(2/3)\alpha]-(1-\alpha)^{2/3}=kt$		Spherical model
First-order (F_1)	$-\ln(1-\alpha)=kt$		
Zero-order (R_1)	$\alpha=kt$	Interfacial Chemical Reaction Mechanism	Reaction-order models
Contracting area (R_2)	$1-(1-\alpha)^{1/2}=kt$		
Contracting volume (R_3)	$1-(1-\alpha)^{1/3}=kt$		

k is the slope of the solid-state kinetic equation, t is the reaction time, and α is conversion rate.

3.2 Determination of solid-state kinetics conversion rate

Figure 1 showed the XRD patterns of specimens mixed with ZnO at 1500, 1510, 1520, 1530, 1540, 1550, and 1560°C for 2, 4, 6, and 8 h respectively. As can be seen from the Fig. 1, the intensity of diffraction peak of $(C,B)_8A_6P$ at 1500-1530°C was very low, and had changed a little with the increase of holding time. And the diffraction peak of CA was obvious, suggesting that the transformation from CA to $(C,B)_8A_6P$ was difficult within the range of calcination temperatures. However, as the calcination temperature increased, the peak intensity of $(C,B)_8A_6P$ increased significantly while the peak intensity of CA decreased dramatically with the calcination temperature ranging from 1540 to 1560°C, which indicated the calcination temperature range of 1540-1560°C was more beneficial to the formation of $(C,B)_8A_6P$.

Standard curves should be established for quantitative analysis using XRD internal standard method. In this experiment, specimen calcined at 1560 °C for 8 h was regarded as standard specimen with 100% conversion rate. Then, 20%, 40%, 60% and 80% standard specimen was mixed with 40% ZnO for XRD analysis, respectively. The results were shown in Fig. 2. The diffraction peak of $(C,B)_8A_6P$ mixed with ZnO at 23.62° was compared with that of ZnO at 36.3°, then the standard curves was established according to

the ratio of the two diffraction peaks intensity for the subsequent quantitative analysis. The results were shown in Fig. 3.

The conversion rate of specimens at elevated temperatures ranged from1500 to 1560°C with the holding time of 2, 4, 6 and 8 h was given in Table 2 and Fig. 4. By comparing the characteristic peak area of XRD patterns, the conversion rate of specimens at different temperature for different holding time was determined. It can be seen that the conversion rate of $(C,B)_8A_6P$ changed a little with an increasing holding time, and it was not exceed 0.5 with the holding time of 8 h and the calcination temperature ranging from 1500 to 1530°C. Furthermore, as a transition calcination temperature region of 1530 to 1540°C, the conversion rate increased sharply at elevated temperatures ranged from 1530 to 1540°C. In addition, the conversion rate was more than 0.8 with the holding time of only 2 h when the temperature ranged from 1540 to 1560°C, and it reached 0.995 with the holding time of 8 h, which indicated that higher calcination temperature as well as holding time had a significant effect on the formation of $(C,B)_8A_6P$ mineral.

Table 2

Conversion rate of specimens at 1500-1560°C for different heat preservation times

	1500°C	1510°C	1520°C	1530°C	1540°C	1550°C	1560°C
2h	0.2	0.236	0.29	0.284	0.802	0.833	0.901
4h	0.236	0.255	0.36	0.372	0.843	0.875	0.95
6h	0.246	0.271	0.39	0.402	0.875	0.899	0.974
8h	0.27	0.297	0.43	0.455	0.904	0.931	0.995

3.3 Dynamic model fitting

The conversion rate α determined by internal standard method at different temperature for different heat preservation times was substituted into the solid-state reaction kinetic mechanism and model formula given in Table 1. Then, the relationship between conversion rate α and holding time T was obtained and the least square method principle was adopted for linear regression analysis. The line regression coefficient reflects the degree of linear correlation, so the determination coefficient more closed to 1 meant the better fitting results. The data of all temperatures was fitted in Origin and the results was shown in Fig. 5. The slopes of lines were the reaction rate constants.

The determination coefficient R^2 of fitting lines was given in Fig. 6. It can be seen that the highest determination coefficient can be observed for model D_2 (2-D diffusion), D_3 (Jander equation) and D_4 (Ginstling equation) at 1500, 1510, 1520 and 1530°C, which indicated the regression model fitting results was optimal in this temperature range. Meanwhile, in terms of model F_1, R_1, R_2 and R_3, the determination

coefficient in this temperature range was also higher. However, the low conversion rate indicated the difficulty in the formation of $(C,B)_8A_6P$ mineral. The reaction may be controlled by multiple processes simultaneously, and the diffusion rate was lowest. The $(C,B)_8A_6P$ mineral was formed on the surface of CA-TCP (interfacial chemical reaction), and then crystal nucleus was formed and grow into small grains (nucleation and growth) or reactant diffused through the product layer and penetrated into the unreacted region (diffusion process). In comparison, the reaction was mainly controlled by diffusion process and had the best fitting results with the Jander equation. The kinetic model of Jander equation [32] assumes that the reactants are the equal-diameter spheres. One reactant is surrounded by the other, and they are in full contact with the products. The reaction proceeds from the surface to the center and contacts in parallel-plate mode, and the thickness of products layer is proportional to the time. This model is suitable for low conversion rates.

At 1540°C, the Ginstling equation (D_4) had the highest determination coefficient (R^2=0.99531) and the interfacial chemical reaction (R_3) had a higher determination coefficient (R^2=0.99423). The same case also applied to 1550 and 1560°C. The conversion rate of $(C,B)_8A_6P$ mineral was higher, and it was more than 90% with the holding time of 8 h at 1540-1560°C. The reaction kinetics of the formation of $(C,B)_8A_6P$ mineral at this stage should be also controlled by diffusion, but it had the best fitting results with the Ginstling equation, which assumed that the product layer was a spherical shell instead of a plane after the reaction began.

The corresponding reaction rate at each temperature was shown in Fig. 7. It can be observed that the reaction rate was no more than 9.4×10^{-7} at 1500-1530°C. Especially, the reaction rate was only 2.1×10^{-7} at 1500°C, and the reaction rate had changed a little with the increase of temperature in this range. Nevertheless, the reaction rate increased sharply at elevated temperatures ranged from 1530°C to 1540°C. Subsequently, as the calcination temperature increased, the reaction rate increased gradually and reached 5.5×10^{-6} at 1560°C, increasing by more than an order of magnitude compared with initial reaction rate. This was consistent with what the conversion rate performed at different temperature ranges.

3.4 Solid-state reaction activation energy

The relationship between reaction rate and thermodynamic temperature is usually described by the Arrhenius equation (The natural logarithmic form of Arrhenius equation is presented here):

$$\ln k = \ln A - Ea/RT$$

where k is the slope of the kinetic equation, A is the preexponential factor, Ea is apparent activation energy ($KJ \cdot mol^{-1}$), R is the ideal gas constant (8.314J / (mol · K)), and T is the thermodynamic temperature.

Due to the solid-state reaction mechanism between 1500-1530°C and 1540-1560°C was different, the activation energy in two temperature ranges should be calculated respectively. The reaction rate constant k and thermodynamic temperature T were listed in Table 3. It can be concluded from the slope of two

lines (Fig. 8) that the activation energy of $(C,B)_8A_6P$ mineral was 1310 and 324 KJ · mol^{-1} at 1500-1530°C and 1540-1560°C, respectively.

Table 3

Reaction rate *k* and thermodynamic temperature *T* at 1500-1560°C

t (°C)	*T* (K)	*k* (S^{-1})
1500	1773.15	2.1×10^{-7}
1510	1783.15	4.8×10^{-7}
1520	1793.15	8.0×10^{-7}
1530	1803.15	9.4×10^{-7}
1540	1813.15	4.4×10^{-6}
1550	1823.15	4.8×10^{-6}
1560	1833.15	5.5×10^{-6}

4. Conclusions

In this work, the internal standard method was performed to evaluate the effects of calcination temperature and holding time on the formation of $(C,B)_8A_6P$ mineral. Meanwhile, the most suitable solid-state kinetic reaction model at each calcination temperature was determined by comparing determination coefficient, which could provide useful information on the preparation of barium-calcium phosphoaluminate cement clinker. The key conclusions from the study were as follows:

1. The conversion rate of $(C,B)_8A_6P$ mineral was less than 0.5 with the holding time of 8 h when the calcination temperature ranged from 1500°C to 1530°C. Once entering the transition temperature range from 1530 to 1540°C, it increased sharply regardless of the holding time.
2. Calcination temperature had a significant effect on the formation of $(C,B)_8A_6P$ mineral, and the optimal calcination temperature for $(C,B)_8A_6P$ mineral sintering ranged from 1540°C to 1560°C, during which the conversion rate was beyond 0.8 with the holding time of only 2 h.
3. The reaction rate of $(C,B)_8A_6P$ mineral was less than 9.4×10^{-7} when the calcination temperature ranged from 1500 to 1530°C, but it reached 5.5×10^{-6} at 1560°C through transition range from 1530 to 1540°C, increasing by more than an order of magnitude compared with initial reaction rate.
4. The Jander equation was feasible for the formation of $(C,B)_8A_6P$ with activation energy of 1310 kJ • mol^{-1} when the temperature ranged from1500 to 1530°C, while the Ginstling equation was feasible

for use with activation energy of 324 kJ • mol^{-1} when the temperature ranged from 1540 to1560°C.

Declarations

Funding

Natural Science Foundations of China-Shandong Joint Fund (No. U1806222), Natural Science Foundations of China (52072149), the Taishan Scholars Program, Case-by-Case Project for Top Outstanding Talents of Jinan. Also, supports from the 111 Project of International Corporation on Advanced Cement-based Materials (No. D17001) is greatly appreciated. The authors declare that no funds, grants, or other support were received during the preparation of this manuscript.

Competing Interests

The authors certify that they have no conflicts of interest, or affiliations with or involvement in any organisation or entity with any financial interest (such as honoraria ; participation in speakers' bureaus ; memebership, employment, cosultancies, stock ownership, or other equity interest ; and expert testimony or patent-licencing arrangements), or non-financial interest (such as personal relationships, knowlegde or beliefs) in the aterials discussed in this manuscript.

Author contributions

All authors contributed to the study conception and design. The conceptualization, software, methodology and writing original draft were performed by Jungang Yuan. The data curation, validation, formal analysis were performed by Hao Liu and Fengnian Wu. The visualization were finished by Yongbo Huang and Jinghua Yan. The supervision, project administration were carried out by Shoude Wang and the funding were supported by Shoude Wang and Lingchao Lu. All authors commented on previous versions of the manuscript, read and approved the final manuscript.

Data Availability

The datasets generated during and/or analysed during the current study are available from the corresponding author on reasonable request.

References

1. Y. Ruan, T. Jamil, C. Hu, B. Prasad, J. Yu, Constr. Build. Mater. **314**, 125416 (2022)
2. L. Kacimi, A. Simon-Masseron, A. Ghomari, Z. Derriche, J. Hazard. Mater. **137**, 129 (2006)
3. C.D. Popescu, M. Muntean, J.H. Sharp, Cem. Concr. Compos. **25**, 689 (2003)
4. Y.L. Li, M.Y. Han, S.Y. Liu, G.Q. Chen, Build. Environ. **151**, 240 (2019)
5. Y. Wang, H. Lu, J. Wang, Crystals (2020)
6. C. Henriksen, C. Michaux, Hum. Serv. Pers. -- Psychol. 12 (1999)

7. I. Maruyama, A. Teramoto, Cem. Concr. Res. **41**, 380 (2011)
8. Š Keprdová, T. Melichar, V. Černý, Adv. Mater. Res. **923**, 161 (2014)
9. W. Hou, F. He, Z. Liu, Constr. Build. Mater. **289**, 123169 (2021)
10. Y.M. Peng, C. Unluer, J.Y. Shi, Powder Technol. **391**, 344 (2021)
11. S. Li, S. Wang, H. Liu, M. Bharath, S. Zhang, Constr. Build. Mater. **230**, 116817 (2020)
12. J. Yuan, S. Li, J. Yan, S. Wang, L. Lu, X. Cheng, Constr. Build. Mater. **311**, 125320 (2021)
13. H. Liu, S. Wang, Y. Huang, B. Melugiri-Shankaramurthy, S. Zhang, X. Cheng, Constr. Build. Mater. **230**, 117012 (2020)
14. Y. Wang, M. Su, L. Zhang, *Sulphoaluminate Cement (in Chinese)* (Beijing University of Technology Press, Beijing, 1999)
15. I. Teoreanu, M. Muntean, I. Dragnea, (1986)
16. F. Xiuji, Cem. Concr. Res. **26**, 955 (1996)
17. P. Yan, Adv. Cem. Res. **5**, 65 (1993)
18. C. Xin, J. Yu, F. Liu, Y. Yue, J. Chang, Cem. Concr. Res. **27**, 1085 (1997)
19. J. Chang, L. Lu, F. Liu, T. Bing, X. Cheng, J Chin Ceram Soc(in Chinese) 10 (1999)
20. X. Cheng, J. Chang, L. Lu, F. Liu, B. Teng, Cem. Concr. Res. **30**, 77 (2000)
21. J. Chang, X. Cheng, F. Liu, L. Lu, B. Teng, Cem. Concr. Res. **31**, 1999 (2001)
22. Y. Huang, S. Wang, C. Gong, Y. Zhao, L. Lu, J Inorg Organomet Polym **23**, 1172 (2013)
23. P. Zhang, S. Zhang, S. Wang, H. Liu, L. Lu, X. Cheng, J. Therm. Anal. Calorim. **7**, 1 (2018)
24. S. Wang, Y. Liu, S. Yang, X. Fu, X. Cheng, J. Therm. Anal. Calorim. 6, (2019)
25. L. Owolabi, A.R. Adebayo, M. Mahmoud, A. Sultan, J. Nat. Gas Sci. Eng. **92**, 104003 (2021)
26. A. Kotani, H. Hakamata, Y. Hayashi, J. Pharm. Biomed. Anal. **202**, 114165 (2021)
27. C. Zhu, J. Lv, K. Liu, Q. Li, Z. Tang, R. Zhou, W. Zhang, J. Chen, K. Liu, X. Li, X. Zeng, Microchem. J. **168**, 106408 (2021)
28. B.D. Glass, Cs., NovákM., E., and Brown, J. Therm. Anal. (2004)
29. M.J. John, K. Muraleedharan, M.P. Kannan, T.G. De_Vi, Thermochim. Acta **534**, 71 (2012)
30. M. Fundamentals, Inorg. Chem. 17315 (2006)
31. X. Li, Y. Zhang, X. Shen, Q. Wang, Z. Pan, Cem. Concr. Res. **55**, 79 (2014)
32. J. Drábiková, S. Fintová, P. Ptáček, I. Kuběna, M. Březina, J. Wasserbauer, P. Doležal, F. Pastorek, Surf. Coatings Technol. **399**, 126101 (2020)

Figures

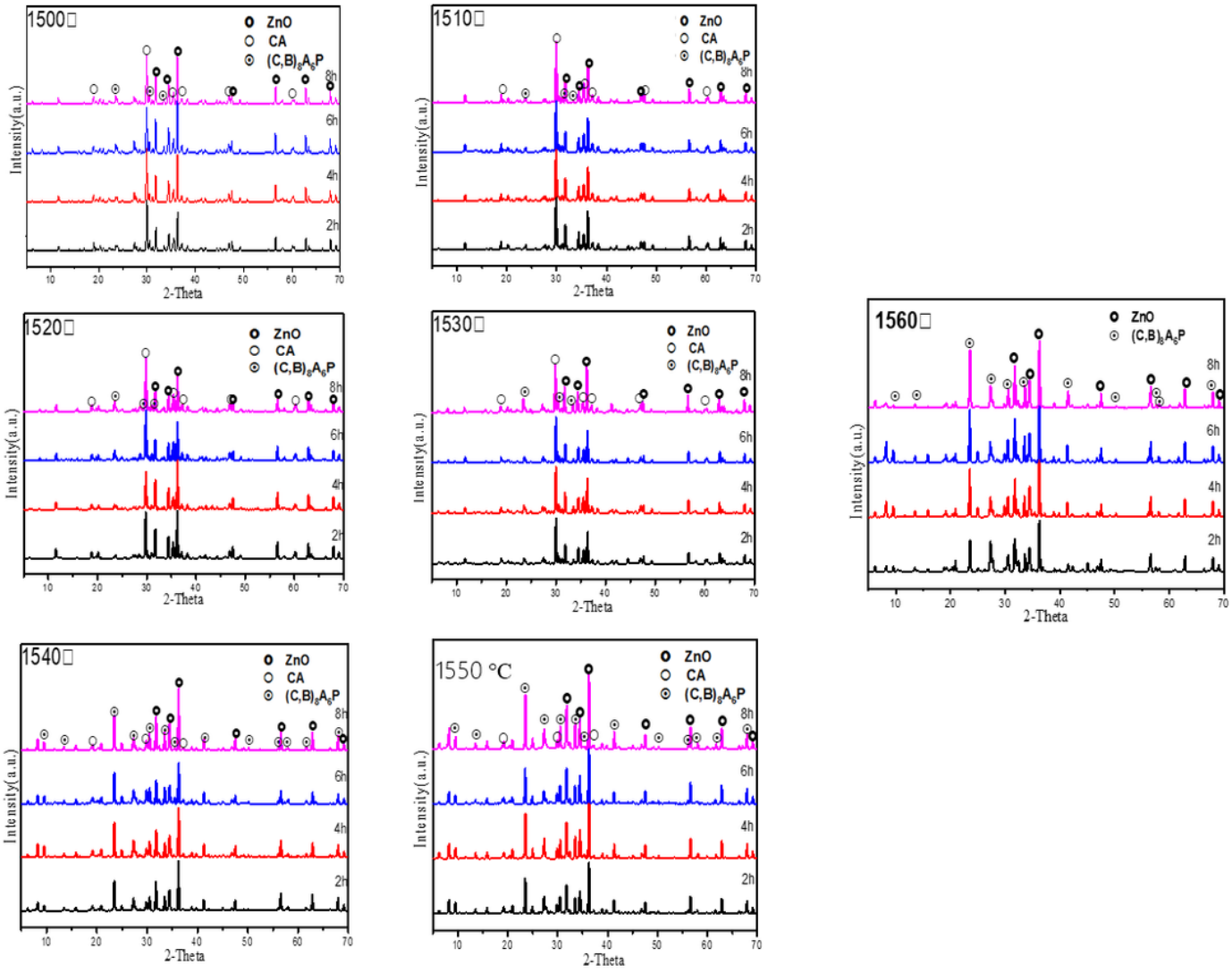

Figure 1

XRD diffraction patterns of specimens at different temperature for different heat preservation times for quantitative analysis

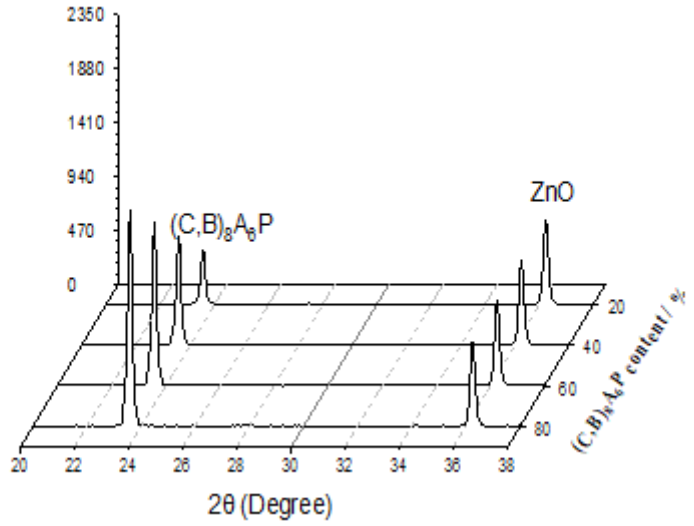

Figure 2

XRD patterns of mixtures composed of 40% ZnO

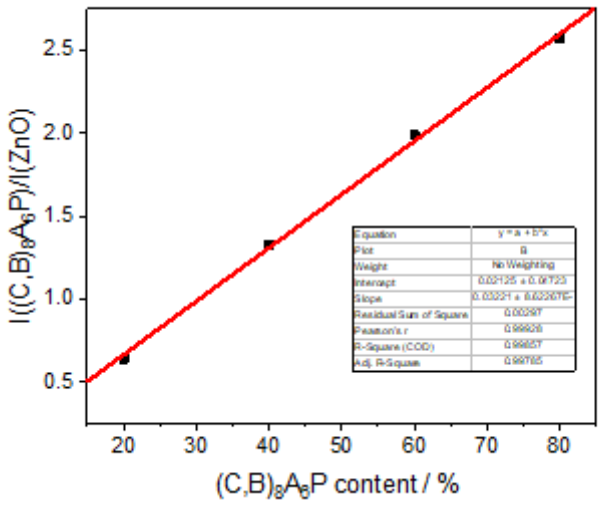

Figure 3

Standard curves obtained by quantitative analysis of mixtures

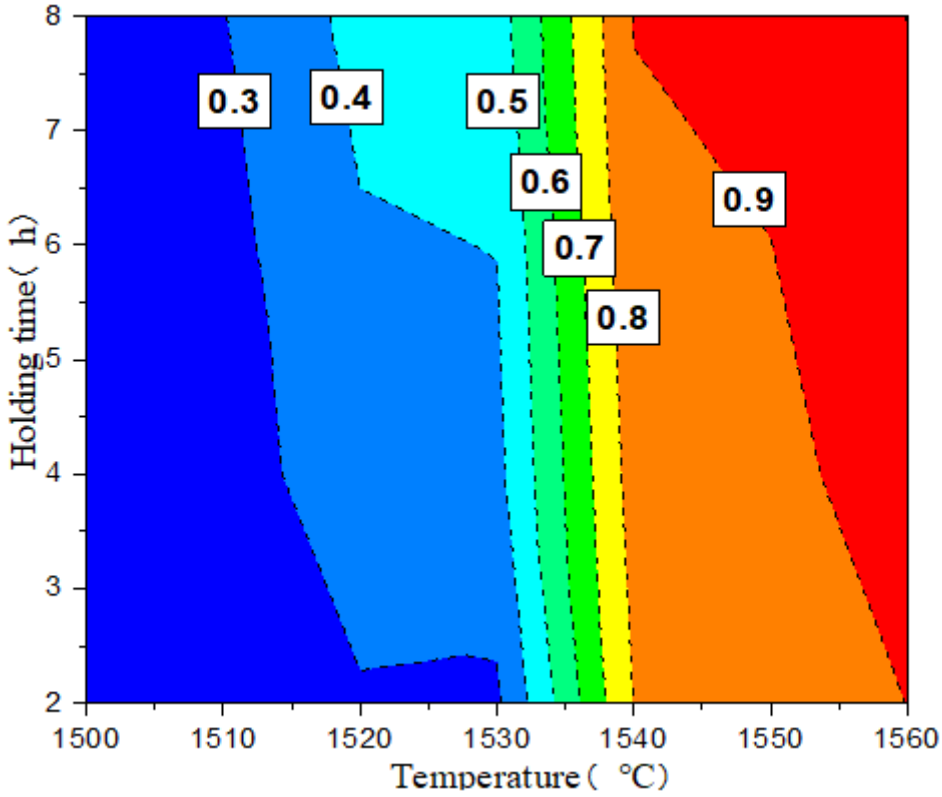

Figure 4

Conversion rate of specimens at 1500-1560 °C with different holding time

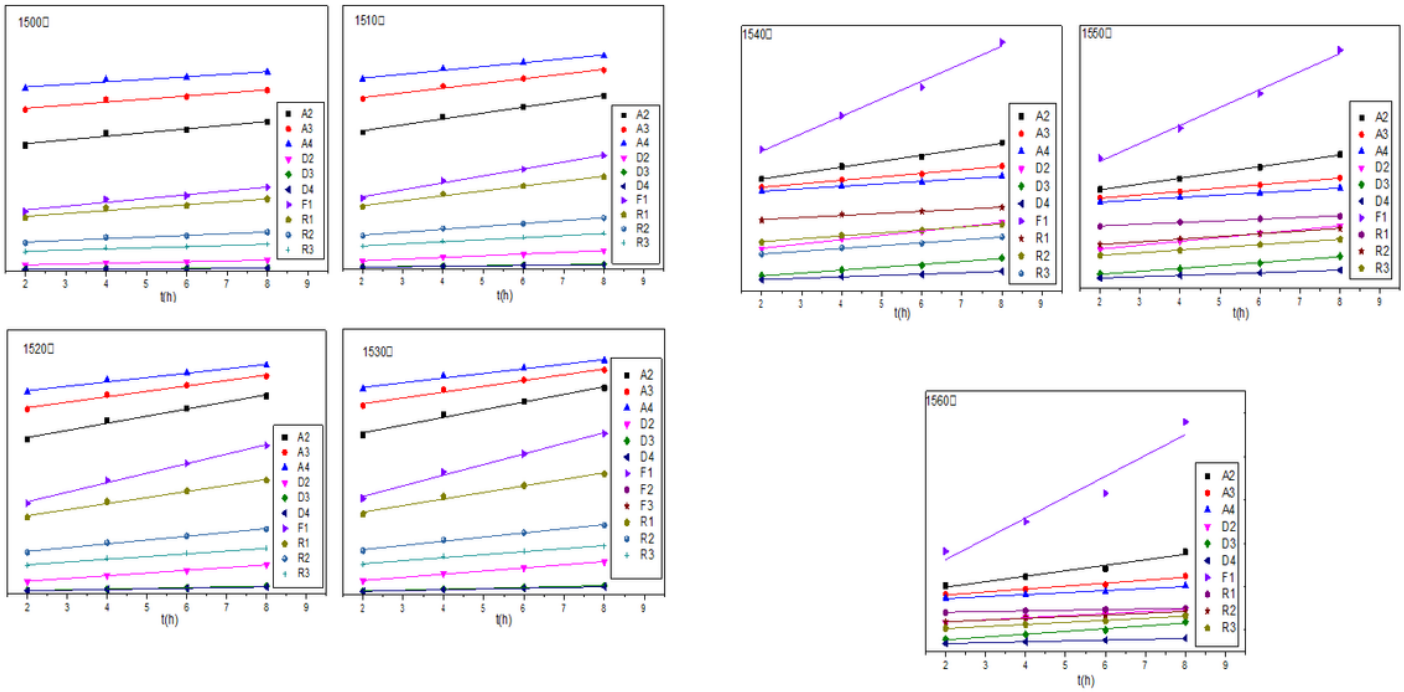

Figure 5

Fitting lines of the dynamic equations at different temperatures

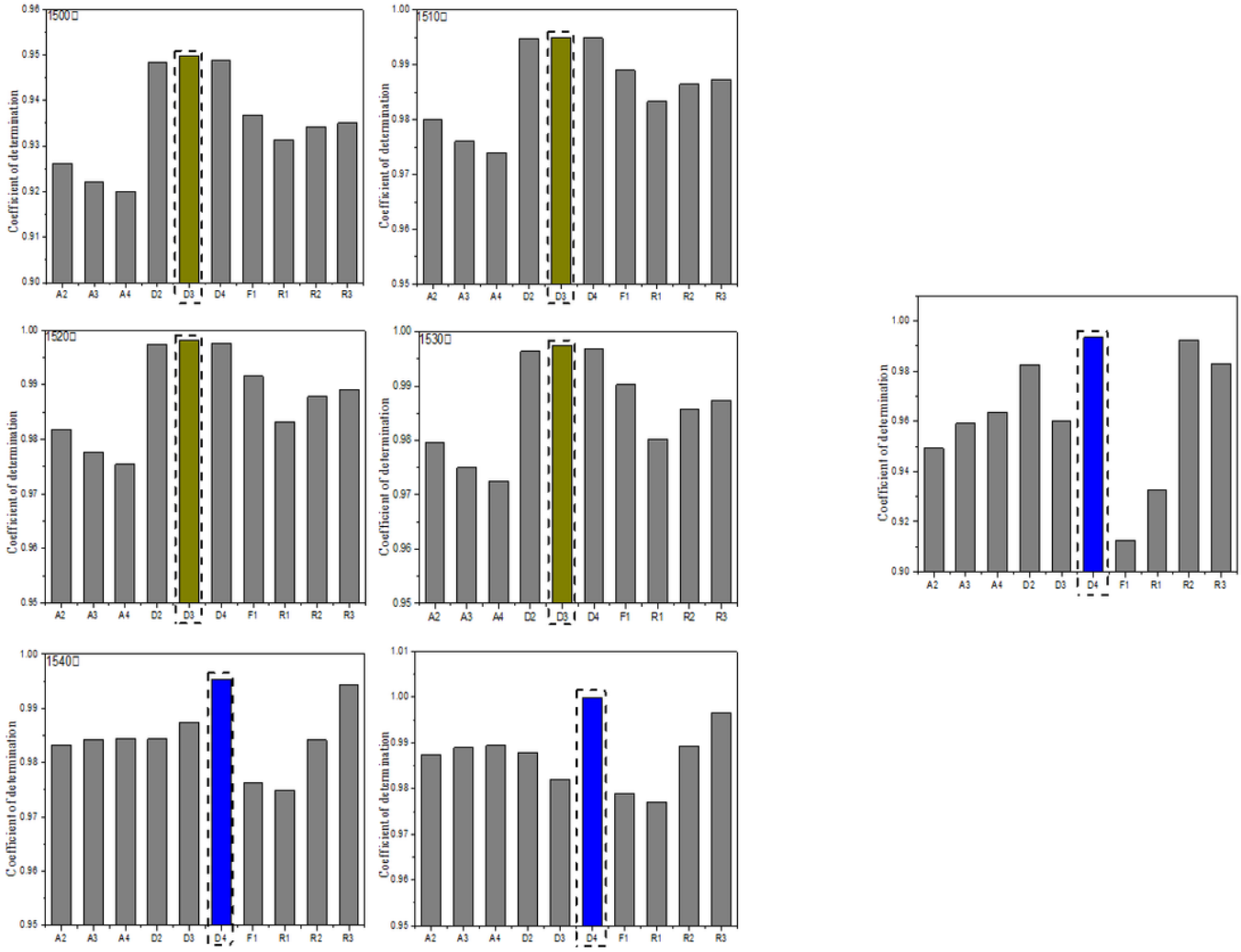

Figure 6

Determination coefficient of kinetic equation at different temperature.

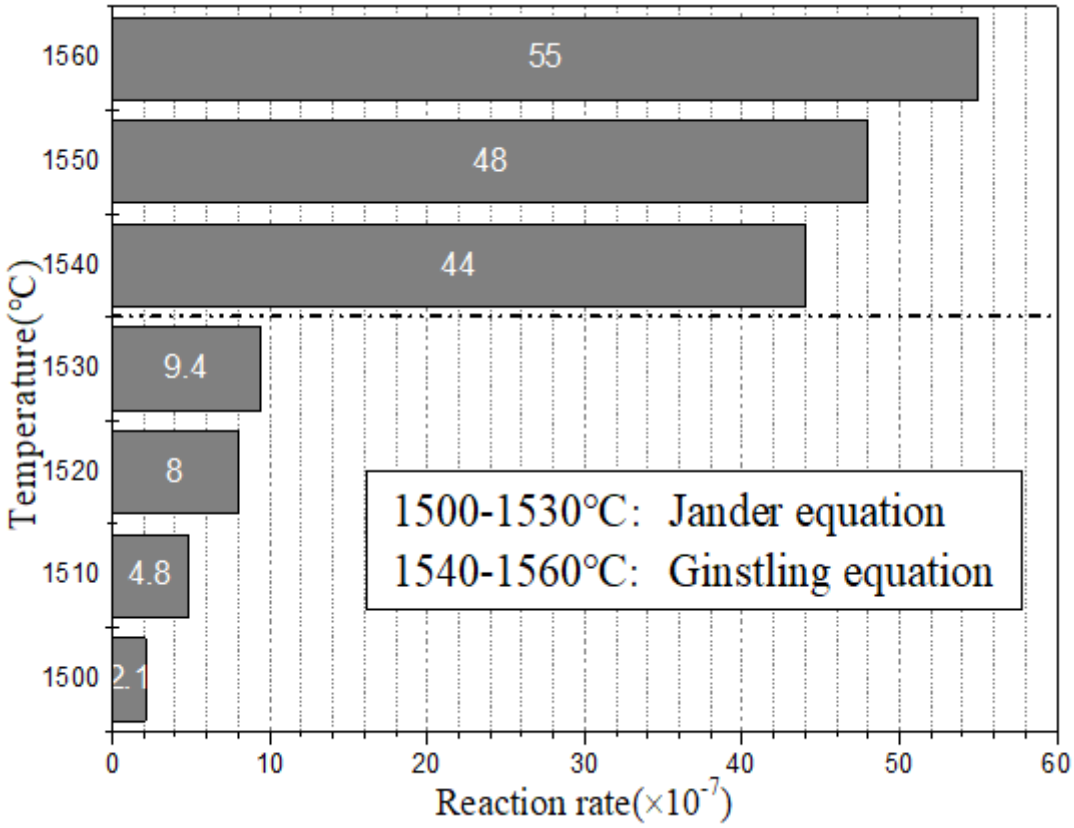

Figure 7

Reaction rate at different temperature

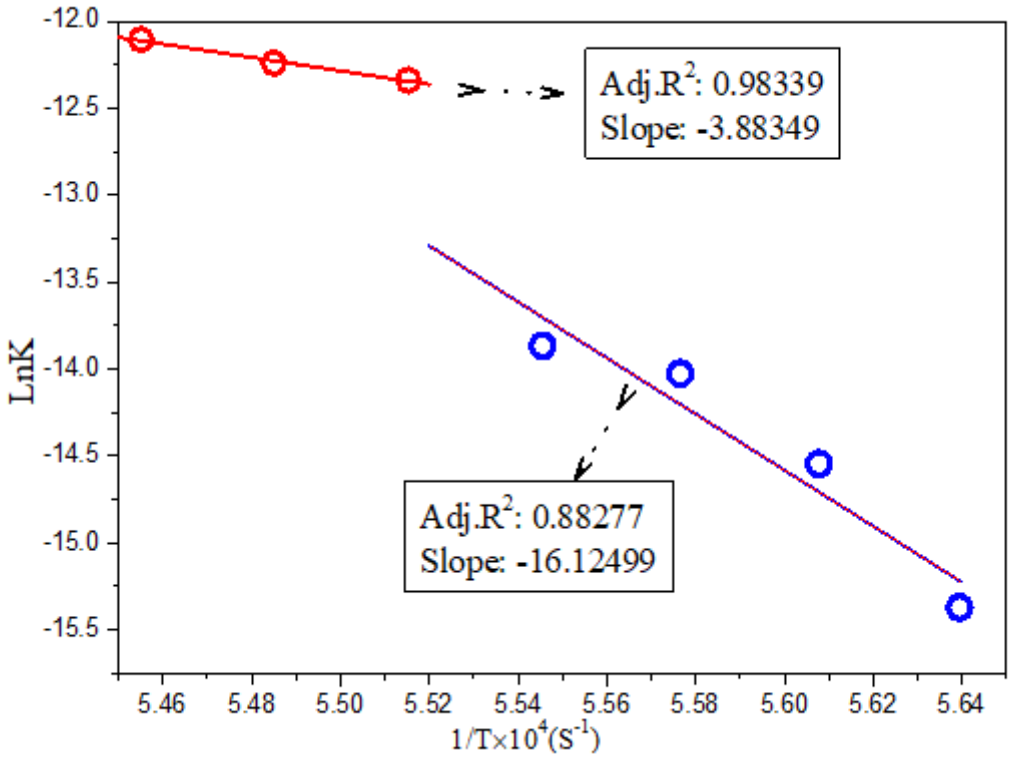

Figure 8

Linear fitting of ln$k$ and 1/T